

# Synchronization and subradiance as signatures of entangling bath between superconducting qubits

Marco Cattaneo,<sup>1,2</sup> Gian Luca Giorgi,<sup>1</sup> Sabrina Maniscalco,<sup>2,3</sup> Gheorghe Sorin Paraoanu,<sup>3</sup> and Roberta Zambrini<sup>1</sup>

<sup>1</sup>*Instituto de Física Interdisciplinar y Sistemas Complejos IFISC (CSIC-UIB),  
Campus Universitat Illes Balears, E-07122 Palma de Mallorca, Spain*

<sup>2</sup>*QTF Centre of Excellence, Turku Centre for Quantum Physics,  
Department of Physics and Astronomy, University of Turku, FI-20014 Turun Yliopisto, Finland*

<sup>3</sup>*QTF Centre of Excellence, Department of Applied Physics,  
School of Science, Aalto University, FI-00076 Aalto, Finland*

(Dated: May 28, 2022)

A common environment acting on two superconducting qubits can give rise to a plethora of phenomena, such as the generation of entanglement between the qubits that, beyond its importance for quantum computation tasks, also enforces a change of strategy in quantum error correction protocols. Further effects induced by a common bath are quantum synchronization and subradiance. Contrary to entanglement, for which full-state tomography is necessary, the latter can be assessed by detection of local observables only. In this work we explore different regimes to establish when synchronization and subradiance can be employed as reliable signatures of an entangling common bath. Moreover, we address a recently proposed measure of the collectiveness of the dynamics driven by the bath, and find that it almost perfectly witnesses the behavior of entanglement. Finally, we propose an implementation of the model based on two transmon qubits capacitively coupled to a common resistor, which may be employed as a versatile quantum simulation platform of the open system in general regimes.

## I. INTRODUCTION

Superconducting qubits are among the best candidates in the race for the creation of a quantum computer [1–3]. Within this challenge, one of the major obstacles is represented by the unavoidable presence of noise [2, 4–7], which induces dissipation and decoherence and breaks all the most fundamental quantum features, such as superposition or entanglement. In order to improve the computational performance, it is very important to know and understand the nature of the noise affecting the qubits during a given experiment. In this paper we address *correlated dissipative noise* induced by a common bath, i.e. by an environment which acts jointly on the qubits. This type of noise appears inevitably due to the coupling to the electromagnetic modes of the nearby waveguides, resonators, and other circuit elements [8, 9]. Its investigation has been receiving more and more interest in the recent past; for example, the two-qubit spectroscopy of spatiotemporally correlated noise between two superconducting qubits has been recently proposed [10]. The interest in correlated noise is motivated e.g. by its detrimental effects on the performance of quantum error correction protocols [11], which must be correspondingly modified [12–26]. A key factor that we must take into account is the generation of qubit-qubit entanglement due to the action of the common bath [27]. In particular, we are not interested in the presence of entanglement in the steady-state, but on the actual possibility that entanglement between the qubits may appear during the evolution, and then decrease toward zero at infinite time. Indeed, this is the phenomenon playing a central role in quantum error correction protocols, that may even improve their performance compared to the case with uncorrelated noise [18, 28, 29].

In order to detect and understand the emergence of bath-mediated transient entanglement during the evolution, we must rely on a measurable figure of merit able to capture its features. The standard entanglement measures require com-

plete state tomography [30, 31]. On the contrary, in this paper we propose to focus on the dynamical properties of the open system in order to identify *local signatures* of entanglement generation. In particular, we address quantum synchronization [32] and subradiance [33, 34], which is a complementary effect of superradiance [35]. Despite its fragility against local noise, subradiance, which manifests itself through the emergence of a slowly-decaying collective mode in the atomic emission, has been reported in different experiments, see for instance Refs. [36–39]. Furthermore, while the presence of a slowly-decaying collective mode is a patent manifestation of subradiance, in the case of only two qubits superradiance does not exhibit a clear enhancement of the emission power [35]. For these reasons, in this work we choose to employ subradiance as signature of an entangling bath.

Contrary to the entanglement measures, both synchronization and subradiance offer the advantage that they can be detected by the observation of some local observables only. Therefore, it is our aim to compare these two phenomena with entanglement generation in several scenarios, in order to understand in which regimes the former may be used as reliable signatures of the latter. This would be particularly useful e.g. in the situations in which the full state tomography is not accessible. In order to achieve this, we need to introduce a measure of quantum synchronization and subradiance which captures their essence and, at the same time, can be computed through simple measurements in a real experiment. We propose such figures of merit and compare them with the maximal entanglement created during the evolution by the common bath, exploring different scenarios and ranges of parameters. We expect synchronization and subradiance to be good signatures if, when varying the relevant parameters of the model, the behavior of their measures follows the one of entanglement. If so, one would be able to enhance or decrease the entanglement production in a given platform of superconducting qubits by only monitoring, for instance, synchroniza-

tion, when changing some relevant experimental conditions. Furthermore, we compare the results with a measure of the ‘‘collectiveness’’ of the dynamics [25] in order to understand whether or not there is a clear, monotonic relation between the strength of these phenomena and the spatial correlations induced by the bath. This measure has been tested in a recent experiment [40].

Our findings suggest a novel application of quantum synchronization for quantum tasks. Recently, transient synchronization was reported to allow for probing of the spectral density of a single qubit immersed in a dissipative environment [41]. Different forms of synchronization have also been reported as beneficial for atomic clocks operation [42, 43]. Besides, we propose to test our predictions by an experimental implementation involving superconducting transmon qubits and resistors. Such scheme represents a versatile simulation platform for quantum thermodynamics [44]. This platform could also be implemented as one of the first experimental realizations of quantum synchronization [45–47].

The paper is structured as follows: Sec. II presents the model and discusses the system dynamics starting from the master equation of the two qubits, while we introduce and analyse the measures of each phenomenon in Sec. III. We discuss the results in Sec. IV, drawing a comparison between the phenomena for several scenarios in Sec. IV A, and proposing an experimental implementation in Sec. IV B, where we also provide the simulation of the system dynamics in a specific case. Finally, we draw some concluding remarks in Sec. V.

## II. MODEL

In order to characterize the collective dissipation effects, we consider two superconducting transmon qubits [8] embedded in a common bath. The qubits frequencies can be different, reflecting either the inherent variability due to fabrication imperfections or the intentional detuning achieved by applying bias magnetic fields. In order to identify the effects induced by a collective environment, we focus on a set-up in which the qubits are not directly interacting, as this could mask the collective origin of dissipative effects. The Hamiltonian of the overall system reads:

$$H = H_S + \sum_k \hbar \Omega_k b_k^\dagger b_k + \mu \sum_k (g_1 \sigma_1^x + g_2 \sigma_2^x) f_k (b_k + b_k^\dagger), \quad (1)$$

where we have introduced the system Hamiltonian  $H_S = \frac{\hbar \omega_1}{2} \sigma_1^z + \frac{\hbar \omega_2}{2} \sigma_2^z$ , with eigenvectors  $|gg\rangle, |ge\rangle, |eg\rangle, |ee\rangle$ . Here,  $|e\rangle$  and  $|g\rangle$  are respectively the excited and the ground state of a qubit,  $\omega_1$  and  $\omega_2$  are the frequencies of respectively the first and second qubit, while the dimensionless coefficients  $g_1$  and  $g_2$  express the weights of the dissipative coupling of each qubit. The parameter  $\mu$  is the coupling constant in the units of energy, while each  $f_k$  is a real dimensionless number representing the strength of the coupling of the  $k$ -th mode of the bath to the qubits. The weak-coupling condition reads  $\omega_1, \omega_2 \gg \mu/\hbar$ .

Motivated by the experimental decay observed in transmon qubits (see e.g. Ref. [7]), we assume that the system follows a Born-Markov master equation [48], and also allow for an additional phenomenological local bath on each qubit, inducing local dissipation characterized by the time  $T_1$ . More details can be found in Appendix A. With these prescriptions, the state of the two-qubit system  $\rho_S$  obeys the master equation [49]

$$\frac{d}{dt} \rho_S(t) = \mathcal{L}[\rho_S(t)] = -i[H_S + H_{LS}, \rho_S(t)] + \mathcal{D}[\rho_S(t)], \quad (2)$$

where  $H_{LS}$  is the Lamb-shift Hamiltonian which reads

$$H_{LS} = \sum_{j,k=1,2} (s_{jk}^\downarrow \sigma_k^+ \sigma_j^- + s_{jk}^\uparrow \sigma_k^- \sigma_j^+), \quad (3)$$

while  $\mathcal{D}$  is the *dissipator* defined as:

$$\begin{aligned} \mathcal{D}[\rho_S] = & \sum_{j,k=1,2} \gamma_{jk}^\downarrow \left( \sigma_j^- \rho_S \sigma_k^+ - \frac{1}{2} \{ \rho_S, \sigma_k^+ \sigma_j^- \} \right) \\ & + \sum_{j,k=1,2} \gamma_{jk}^\uparrow \left( \sigma_j^+ \rho_S \sigma_k^- - \frac{1}{2} \{ \rho_S, \sigma_k^- \sigma_j^+ \} \right). \end{aligned} \quad (4)$$

The coefficients of the master equation (2) contain both a contribution coming from the common bath, introduced in Eq. (1), and a contribution proportional to  $1/T_1$ , i.e. due to the phenomenological local bath acting on each qubit. Their form can be found in Appendix A.

The solution of the master equation is obtained by finding the eigenvalues together with the right and the left eigenvectors of the Liouvillian  $\mathcal{L}$ , and from now on we assume that the latter is diagonalizable. As discussed in Appendix B, thanks to a symmetry of the master equation we can divide the Liouvillian superoperator into five blocks [50], which we label using the subscript  $d$  such that  $d = -2, -1, 0, 1, 2$ :  $\mathcal{L} = \bigoplus_{d=-2}^2 \mathcal{L}_d$ . The blocks have respectively dimension  $1, 4 \times 4, 6 \times 6, 4 \times 4, 1$ , and two of them can be trivially obtained from the others:  $\mathcal{L}_{-1} = \mathcal{L}_1^*$ ,  $\mathcal{L}_{-2} = \mathcal{L}_2^*$  (see Appendix B for details). We name the eigenvalues of the block  $\mathcal{L}_d$  as  $\{\lambda_j^{(d)}\}_{j=1}^{\sqrt{\dim(\mathcal{L}_d)}}$ , the right eigenvectors as  $\{\tau_j^{(d)}\}_{j=1}^{\sqrt{\dim(\mathcal{L}_d)}}$  and the left eigenvectors as  $\{\tilde{\tau}_j^{(d)}\}_{j=1}^{\sqrt{\dim(\mathcal{L}_d)}}$ . The latter are normalized such that  $\text{Tr}[(\tilde{\tau}_j^{(d)})^\dagger \tau_k^{(d)}] = \delta_{jk}$ , where  $\langle O_1, O_2 \rangle = \text{Tr}[O_1^\dagger O_2]$  is the Hilbert-Schmidt inner product of the space of operators acting on the system (see e.g. Ref. [51]). Using this notation and the master equation (2), the state of the system at time  $t$  is readily obtained:

$$\rho_S(t) = \bigoplus_{d=-2}^2 \sum_{j=1}^{\sqrt{\dim(\mathcal{L}_d)}} p_{0j}^{(d)} \tau_j^{(d)} \exp(\lambda_j^{(d)} t), \quad (5)$$

where  $p_{0j}^{(d)} = \text{Tr}[(\tilde{\tau}_j^{(d)})^\dagger \rho_S(0)]$  defines the initial conditions. Eq. (5) represents the *normal modes decomposition* of the open dynamics of the system.

### III. FIGURES OF MERIT OF COLLECTIVE PHENOMENA

Next, we introduce the figures of merit of synchronization, subradiance, entanglement generation and correlations induced by the presence of a common bath during the relaxation dynamics of the two qubits and comment on their experimental characterization.

#### A. Quantum synchronization

The emergence of transient synchronized dynamics of local observables has been predicted in different quantum systems in the recent years [43, 52–65]. This phenomenon is induced by some forms of dissipation into an environment (see for instance Refs. [32, 66] for a review), and in some instance it can persist asymptotically [53, 59, 65]. Other forms of synchronization in the quantum regime have also been explored, as entrainment in presence of an external driving or synchronization among self-sustained oscillators [67–69], with the latter phenomenon favored by collective dissipation as recently shown for optomechanical systems [58]. For the purpose of this work we focus on transient spontaneous synchronization mediated by the bath. Taking  $\sigma_1^x(t)$  and  $\sigma_2^x(t)$  as local observables, their dynamics can be completely recovered by analyzing the Liouvillian block  $\mathcal{L}_1$  only [50, 51]:

$$\langle \sigma_k^x(t) \rangle = \sum_{j=1}^4 2 \left| p_{0j}^{(1)} c_{jk}^{(1)} \right| e^{\text{Re}(\lambda_j^{(1)})t} \cos\left(\text{Im}(\lambda_j^{(1)})t + \varphi_{jk}^{(1)}\right), \quad (6)$$

with  $c_{jk}^{(1)} = \text{Tr}\left[\sigma_k^x \tau_j^{(1)}\right]$  and  $\varphi_{jk}^{(1)} = \arg(p_{0j}^{(1)} c_{jk}^{(1)})$ . Here,  $\text{Re}(\lambda_j^{(1)})$  and  $\text{Im}(\lambda_j^{(1)})$  denote the real and imaginary parts of the eigenvalue  $\lambda_j^{(1)}$ .

A well-known figure of merit to detect the synchronized dynamics of two observables is the Pearson coefficient [32], whose definition can be found in Eq. (C1) of Appendix C. Being a temporal correlation of the measured coherences dynamics of each qubit, this quantity can be experimentally measured. For our theoretical analysis in different parameter regimes we introduce a time-independent figure of merit. This will only depend on the coefficients of the master equation (2) and the initial conditions. In fact, the emergence of synchronization is due to a mode of the block  $\mathcal{L}_1$  (let us say the one with eigenvalue  $\lambda_4^{(1)}$ ) decaying much slower than any other mode [52, 53, 55]. According to Eq. (6), at a certain time  $t_S$ ,  $\sigma_1^x(t)$  and  $\sigma_2^x(t)$  will synchronize at frequency  $\text{Im}(\lambda_4^{(1)})$ . A measure of synchronization can be introduced as follows:

$$Syn = \left| \frac{\log 100}{t_S \text{Re}(\lambda_4^{(1)})} \right|. \quad (7)$$

$Syn$  describes the ratio between the decay time of the slowest-decaying mode  $\lambda_4^{(1)}$  and the *synchronization time*  $t_S$ .

Then,  $Syn > 1$  indicates that synchronization appears before the “relaxation” of the slowest decaying mode. The bigger  $Syn$ , the more detectable the synchronization in the system. We choose  $\rho_S(0) = |\psi_{Syn}\rangle \langle \psi_{Syn}|$ , as initial state of the evolution, where  $|\psi_{Syn}\rangle = (\cos \pi/4 |e\rangle + \sin \pi/4 |g\rangle) \otimes (\cos \pi/3 |e\rangle + i \sin \pi/3 |g\rangle)$ , as such a state has a large amount of initial coherence and at the same time is not symmetric under the exchange of the two qubits, which avoids pathological behaviors for some choice of parameters due to symmetry.

#### B. Subradiance

In order to introduce a measure able to capture the appearance of subradiance in our model, we focus on the observables describing the population of the excited state of each qubit, defined as:

$$\begin{aligned} P_1^e &= |e\rangle \langle e| \otimes \mathbb{I}, \\ P_2^e &= \mathbb{I} \otimes |e\rangle \langle e|. \end{aligned} \quad (8)$$

The dynamics of  $P_1^e$  and  $P_2^e$  can be completely recovered by analyzing the Liouvillian block  $\mathcal{L}_0$  only [50, 51]:

$$\langle P_k^e(t) \rangle = \sum_{j=1}^6 p_{0j}^{(0)} h_{jk}^{(0)} e^{\lambda_j^{(0)} t}, \quad (9)$$

where  $h_{jk}^{(0)} = \text{Tr}\left[P_k^e \tau_j^{(0)}\right]$ .

As said in the introduction, subradiance entails the presence of a slowly-decaying collective mode in the dynamics of both the observables  $P_1^e(t)$  and  $P_2^e(t)$  defined in Eq. (8), which remains alive even when all the other modes have disappeared. As  $\mathcal{L}_0$  always has at least one zero eigenvalue, corresponding to the steady state of the dynamics [50]. We do not consider the latter, and we focus on the remaining five. Analogously to the problem of quantum synchronization, we introduce the measure of subradiance as:

$$Sub = \left| \frac{\log 100}{t_B \text{Re}(\lambda_5^{(0)})} \right|, \quad (10)$$

where  $\lambda_5^{(0)}$  is the slowest-decaying mode of  $\mathcal{L}_0$  (apart from the non-decaying one) and  $t_B$  is the *subradiance time* defined in Appendix C. We assume to start the evolution in the *subradiant state*  $(|eg\rangle - |ge\rangle)/\sqrt{2}$ , which in a perfectly symmetric scenario ( $\omega_1 = \omega_2$ ,  $g_1 = g_2$ ) lives in a decoherence-free subspace.

As  $Sub$  describes the ratio between and the decay time of the slowest-decaying mode  $\lambda_5^{(0)}$  and the subradiance time,  $Sub > 1$  implies that subradiance appears before the “relaxation” of the slowest decaying mode. If we consider the symmetrical scenario leading to a decoherence-free subspace, we have that  $Sub = \infty$ , since the initial state would be a steady state of the evolution. In general terms, the bigger  $Sub$  the more detectable the subradiance in the system.

### C. Entanglement generation

The capability of a common bath to entangle two initially uncorrelated quantum systems has been predicted in several scenarios [27, 70–86] and also demonstrated in some platforms [31, 87, 88]. Following the works by Benatti et al. on Markovian dynamics [75, 81, 89], we can provide sufficient conditions on the capability of the master equation (2) to generate entanglement for given configurations of the Hamiltonian parameters. The conditions are presented in Appendix D.

As a measure of entanglement of the state of the system we choose the *negativity*, which is a well-defined entanglement monotone [90]. It is given by

$$\mathcal{N}(t) = \sum_{r_j(t) < 0} |r_j(t)|, \quad (11)$$

where  $r_j(t)$  are the eigenvalues of the partial transpose of the state of the system  $\rho_S(t)$  with respect to the second qubit.  $\rho_S(t)$  evolves according to the master equation (2), therefore the negativity depends on time as well, and we choose as measure of the entangling power of the bath the maximum value over the whole evolution:

$$\mathcal{N}_M = \sup_{t > 0} [\mathcal{N}(t)]. \quad (12)$$

This definition clearly depends on the initial conditions. As separable initial state of the evolution, we set  $\rho_S(0) = \rho_C = 1/4 \sum_{j,k,l,m=e,g} |jk\rangle \langle lm|$ , which is the maximally coherent state. We choose so by considering that the majority of quantum algorithms start from  $\rho_C$ , given that the latter is obtained by applying a Hadamard gate on the state with all the qubits in 0 (here  $|gg\rangle$ ) [91].

The computation of  $\mathcal{N}_M$  requires the complete knowledge of the state of the system  $\rho_S(t)$  at any time  $t$ . This can be obtained experimentally by means of the full-state tomography [30, 31], based on joint measurements on both the qubits at the same time, which is highly resource-intensive.

### D. Collectiveness of the dynamics

To quantify the collectiveness of the dynamics of two qubits driven by a common bath, we employ a measure recently introduced by Rivas and Müller [25]. It quantifies how much a given quantum evolution  $\mathcal{E}(t)$  of two subparties 1 and 2 differs from a totally uncorrelated dynamics written as  $\mathcal{E}_1(t) \otimes \mathcal{E}_2(t)$ .

The measure is based on the Choi-Jamiołkowski isomorphism which makes use of the state  $|\Psi_{SS'}\rangle$ , living in  $\mathcal{H}_S \otimes \mathcal{H}_{S'}$ , where  $\mathcal{H}_S$  is the Hilbert space of the system and  $\mathcal{H}_{S'}$  a copy of it.  $|\Psi_{SS'}\rangle$  is defined as:

$$|\Psi_{SS'}\rangle = \frac{1}{2} \sum_{j,k=e,g} |jk\rangle_{12} \otimes |jk\rangle_{1'2'}. \quad (13)$$

The subscripts indicate that the generic single-qubit state  $|j\rangle$  refers to the qubit 1 or 2 of  $\mathcal{H}_S$  or to the qubit 1' or 2' of  $\mathcal{H}_{S'}$ . Let us name  $\mathcal{E}(t) = \exp(\mathcal{L}t)$  the quantum map describing the

evolution until time  $t$ . Then, we can introduce a  $16 \times 16$  matrix  $\Phi_{\mathcal{E}}(t)$ , defined by

$$\Phi_{\mathcal{E}}(t) = \mathcal{E}(t) \otimes \mathbb{I}_{S'} [|\Psi_{SS'}\rangle \langle \Psi_{SS'}|]. \quad (14)$$

Since  $\mathcal{E}(t)$  is completely positive,  $\Phi_{\mathcal{E}}(t)$  is positive-semidefinite and has trace 1, i.e. is a state in the Hilbert space  $\mathcal{H}_S \otimes \mathcal{H}_{S'}$ . The measure of correlations in the dynamics  $\bar{I}$  is defined as the normalized quantum mutual information of  $\Phi_{\mathcal{E}}(t)$ :

$$\begin{aligned} \bar{I}(\mathcal{E}(t)) &= \frac{I(\Phi_{\mathcal{E}}(t))}{4 \log 2} \\ &= \frac{S(\text{Tr}_{11'}[\Phi_{\mathcal{E}}(t)]) + S(\text{Tr}_{22'}[\Phi_{\mathcal{E}}(t)]) - S(\Phi_{\mathcal{E}}(t))}{4 \log 2}, \end{aligned} \quad (15)$$

where  $S$  is the von Neumann entropy and  $\text{Tr}_{11'}$  ( $\text{Tr}_{22'}$ ) is the partial trace on the qubit 1 and 1' (2 and 2').  $0 \leq \bar{I}(\mathcal{E}(t)) \leq 1$ , it is null if and only if the dynamics is uncorrelated, and it satisfies a fundamental principle which allows one to consider the correlations in the dynamics as a resource (see Ref. [25] for details), therefore it is a well-defined measure. It can be shown that it reaches the value  $\bar{I}(\mathcal{E}(t)) = 1$  only if  $\mathcal{E}(t)$  is unitary.

$\bar{I}(\mathcal{E}(t))$  is a measure for the correlation in the quantum map that evolves the state until time  $t$ . Since we would like to have a figure of merit independent of time, following the original reference we choose:

$$\bar{I}_M = \sup_{t > 0} [\bar{I}(\mathcal{E}(t))]. \quad (16)$$

For convenience, let us term the measure in Eq. (16) as *collectiveness*. The experimental computation of  $\bar{I}_M$  requires quantum process tomography which is highly non-trivial [40], and in the present work we consider this figure of merit only as an abstract indicator to be compared with the other measures.

## IV. RESULTS

### A. Comparison in different scenarios

Although synchronization, subradiance, entanglement generation and correlations in the dynamics of decoupled qubits share a common origin in this system, namely the presence of a collective bath, they are essentially four different physical phenomena. From a mathematical perspective, this is displayed by the block structure of the Liouvillian superoperator discussed in Appendix B. We observe that quantum synchronization is described by the block  $\mathcal{L}_1$  (Eq. (6)), subradiance by the block  $\mathcal{L}_0$  (Eq. (9)), while both the negativity Eq. (11) and the collectiveness Eq. (15) may in general depend on all the blocks of the Liouvillian. We know that, only in the case with zero temperature, a parametric dependence induces the same separation between the decay rates characterizing synchronization and subradiance [51], but in more general scenarios there is no clear relation between the phenomena, given that

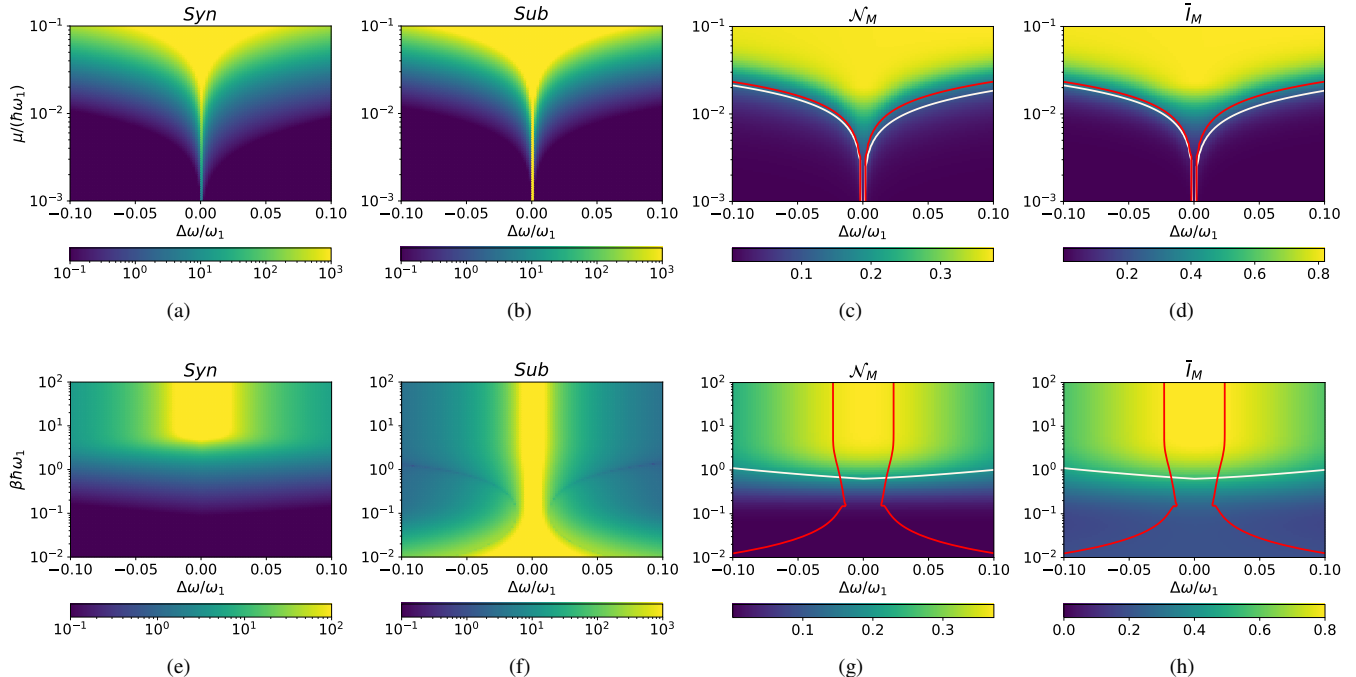


FIG. 1. Measures of quantum synchronization, subradiance, entanglement generation and collectiveness in the balanced scenario ( $g_1 = g_2$ ), varying the detuning  $\Delta\omega = \omega_1 - \omega_2$  and the coupling constant  $\mu$  (figs. (a)-(d)) or the inverse temperature  $\beta$  (figs. (e)-(h)). Having fixed the quantity on the  $y$ -axis, the remaining parameters are set as  $g_1 = g_2 = 1$ ,  $\mu = 10^{-1.5}\hbar\omega_1$ ,  $\beta = 10/\hbar\omega_1$  and  $T_1 = 3 \times 10^5/\omega_1$ . We have chosen an Ohmic spectral density of the environment (see Eq. (A4)). The white line delimits the area in which  $Syn$  is bigger than 1, while the red line delimits the area in which  $Sub$  is bigger than 1 in figs. (c) and (d) and bigger than 100 in figs. (g) and (h).

each Liouvillian block has an independent behavior. Therefore, a deep numerical investigation is needed in order to compare the strength of each phenomenon in different scenarios and their possible concomitance.

In the following, we will explore several situations by studying how the figures of merit vary for different parameters in the two qubits platform introduced in Sec. II. We will analyze their behavior against the detuning, the bath temperature, the system-bath coupling, and the unbalancing of the coupling, also exploring the dependence on initial conditions. For the sake of clarity, we will first discuss the case  $g_1 = g_2$  and then move to the unbalanced case, corresponding to a situation in which collective dissipation acts with different strength on the two qubits. The results are displayed in Fig. 1 for the balanced case  $g_1 = g_2$ , where the four indicators are plotted against the detuning (1(a-d)) and against the temperature (1(e-h)) and in Fig. 2 for the unbalanced case  $g_1 \neq g_2$ . Further results are presented in Fig. 5 of Appendix E. In all the scenarios, anticipating the relevant case for the platform we are going to introduce in Sec. IV B, we set an Ohmic spectral density of the bath (see Eq. (A4)).

### 1. Balanced couplings

Let us start analyzing the role played by the system-bath coupling: the higher the coupling strength, the stronger the effects of the common bath, and therefore the larger the four

measures. This can be observed, for instance, in Figs. 1(a)-(d) and in Figs. 5(e)-(h). If  $\mu$  is too weak, the unitary evolution driven by the system Hamiltonian will play the only relevant role in the dynamics, and no collectiveness, entanglement, synchronization or subradiance will appear. For instance, with the parameters employed in Figs. 1(a)-(d) (i.e.  $g_1 = g_2 = 1$ ,  $\beta = 10/\hbar\omega_1$ ,  $T_1 = 3 \times 10^5/\omega_1$ ), we observe that for  $\mu \lesssim 10^{-2.5}\hbar\omega_1$  and  $\Delta\omega \approx 0.01\omega_1$  neither synchronization nor subradiance emerge before thermalization, while both negativity and collectiveness are negligible.

As for the detuning, in all scenarios,  $\mathcal{N}_M$  and  $\bar{I}_M$  decrease as soon as  $\Delta\omega$  increases, consistently with a vanishing dissipative coupling. Indeed, in spite of the presence of a common bath, in this regime the dynamics can be well approximated by a full secular master equation dominated by local instead of collective dissipation [49]. This also occurs when varying the value of the local relaxation time  $T_1$  (Fig. 5(c)-(d)). As shown in Figs. 1(a)-(b)-(e)-(f), synchronization and subradiance display the same behavior: in Figs. 1(c)-(d) we have drawn a line demarcating the regions of parameters in which  $Syn$  and  $Sub$  are bigger than 1, and the same in Figs. 1(g)-(h) with the difference that the red line indicates a value of  $Sub > 100$ . In Figs. 1(c)-(d) (at fixed inverse temperature  $\beta = 10/\hbar\omega_1$ ) we see that these regions coincide with the ones in which  $\mathcal{N}_M$  and  $\bar{I}_M$  display stronger values. We observe that synchronization shows a slight asymmetry between the scenarios with  $\Delta\omega > 0$  and  $\Delta\omega < 0$ . This is due to the fact that  $Syn$  is particularly sensible to the change of the absolute value of the frequencies

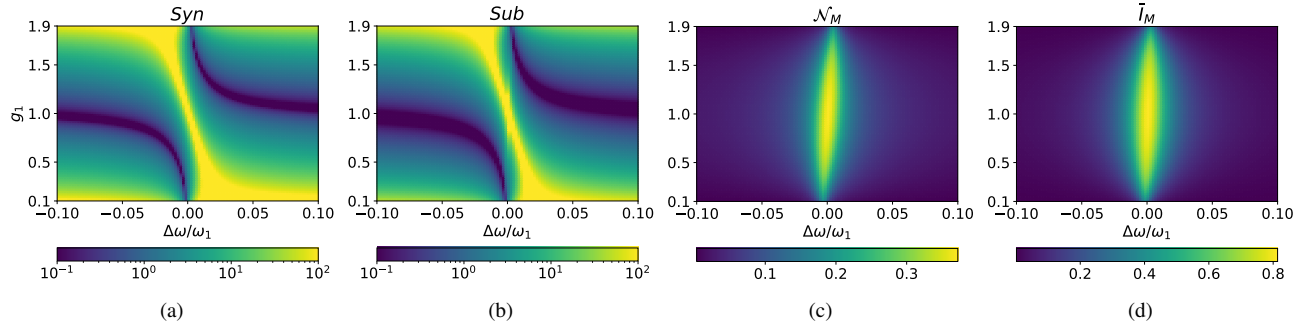


FIG. 2. Measures of quantum synchronization, subradiance, entanglement generation and collectiveness in the presence of an unbalanced coupling of each qubit to the bath. We vary the detuning  $\Delta\omega = \omega_1 - \omega_2$  and the weight of the dissipative interaction  $g_1$  (while  $g_2 = 2 - g_1$ ). The remaining parameters are set as  $\mu = 10^{-2}\hbar\omega_1$ ,  $\beta = 10/\hbar\omega_1$  and  $T_1 = 3 \times 10^5/\omega_1$ . We have chosen an Ohmic spectral density of the environment (see Eq. (A4)).

$\omega_1$  and  $\omega_2$ , and not only of the detuning  $\Delta\omega$ .

## 2. Unbalanced couplings

More complex is the dependence with the temperature as depicted in Figs. 1(e)-(h) and Figs. 5(e)-(h). In this case, the measure of subradiance displays notable differences with respect to the other ones: it is enhanced by higher temperatures, unlike the other phenomena. The fact that, in general, higher temperatures hinder entanglement generation through a common bath has been observed since the first papers on the topic [78]. As for synchronization, in agreement with what was partially discussed in the literature [92, 93], we observe that while a higher temperature speeds up the relevant decay rates (formally the eigenvalues of the block  $\mathcal{L}_1$ , see Eq. (6)), it does not increase the gap between the two slowest eigenvalues. As a consequence, the synchronization time does not change considerably, while the relaxation time occurs way before than at lower temperatures, and then the measure of Eq. (7) decreases. Furthermore, we observe that the collectiveness decreases as well when the temperature increases, although, contrary to the negativity and synchronization, its value never vanishes for  $T \rightarrow \infty$ . Indeed, even at infinite temperature the master equation describing the dynamics driven by a common bath is different from the one driven by two independent local baths. Subradiance displays a radically different behavior, as it increases in the high-temperature regime. This can be understood by considering the perfectly symmetric case with  $\Delta\omega = 0$ , where the subradiant state lives in a decoherence-free subspace, independently of the chosen temperature. In this scenario, the subradiant mode does not decay at any temperature, while the decay rates of all the other ones are speeded up by the increase of temperature. Consequently, the subradiance time is brought forward for higher temperatures. For continuity, we can expect a similar behavior also when the detuning is perturbed. We indeed observe that the slowest decay rate is not significantly affected by the value of the temperature, and thus  $Sub$  is enhanced for higher temperatures.

The maximal collective effect is achieved when the coupling between the qubits and the bath is balanced, i.e.  $g_1 = g_2$ . A less relevant scenario appears when this is not true anymore, and the collectiveness of the evolution inevitably decreases. Let us analyze this case: the bigger the unbalance between the weights of the dissipative coupling  $g_1$  and  $g_2$ , the smaller the collective effects in the dynamics. Indeed, both collectiveness and negativity decrease as the unbalance increases (see Figs. 5(k)-(l) and 2(c)-(d)). If we weaken the coupling of one of the two qubits by varying  $g_1$  and  $g_2$ , we monotonically decrease the values of  $\mathcal{N}_M$  and  $\bar{I}_M$ , reaching zero in the trivial limit  $g_1 \rightarrow 0$ ,  $g_2 \rightarrow 2$ . On the other hand, a significant unbalance between the weights of the dissipative interaction  $g_1$  and  $g_2$  breaks the possibility of using synchronization and subradiance as signatures of entanglement generation. Indeed, the appearance of synchronization and subradiance depends not only on the collectiveness of the evolution, but also on the gap between the eigenvalue of the slowest eigenmode and all the remaining ones. By unbalancing the coupling, we may enhance this gap, and therefore increase the values of  $Syn$  and  $Sub$  (as for instance already discussed in Ref. [41]). This behavior is observed in Figs. 2 and 5(i)-(j), which shows that, by unbalancing  $g_1$  and  $g_2$ , the separation between the eigenvalues of both synchronization and subradiance is enhanced in a stronger way than the collectiveness of the relevant eigenmodes is decreased, and therefore we obtain higher values of  $Syn$  and  $Sub$ . Finally, let us comment that, in the unbalanced scenario, the behavior of synchronization and subradiance when varying the temperature is now completely different from the balanced case (see Figs. 5(i)-(j)). Indeed, the arguments we used in the previous section to understand the behavior of the figures of merit as a function of the temperature are now not valid anymore, and, for example, for some values of  $g_1$  and  $g_2$  we obtain a higher synchronization for higher temperatures.

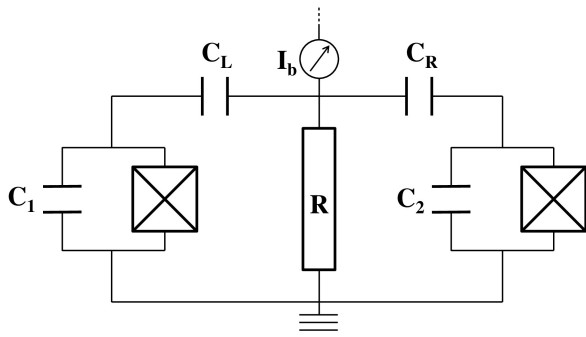


FIG. 3. Circuit diagram representing two transmon qubits, characterized by the capacitances  $C_1$  and  $C_2$ , capacitively coupled to the same resistor  $R$ , respectively through the capacitors  $C_L$  and  $C_R$ . The resistor plays the role of a common bath with Ohmic spectral density, that can be heated up by an external bias current  $I_b$ .

### 3. Dependence on the initial conditions

Let us finally try to understand whether our results depend on the specific initial states we have chosen. In order to do so, for the case of synchronization and subradiance, we have computed a modified form of their figure of merit in which we do not consider the initial conditions. In particular, we have set each  $p_{0j}^{(1)}$  and  $p_{0j}^{(0)}$  equal to 1 in Eqs. (C2) and (C4), and we have computed these slightly modified measures in all the scenario discussed before. We have found that the results without taking into account the initial conditions mimic the ones depicted in Figs. 1, 2 and 5, with no exceptions.

Focusing on the entanglement generation, we can explore different initial conditions by considering the states discussed in Appendix D. We have found that the sufficient conditions for having entanglement at time  $t \rightarrow 0^+$  starting from a given initial state, actually can be associated to the behavior of the entanglement generation throughout the whole evolution. For instance, we observe that no entanglement is generated by the bath when starting the dynamics in the pure states  $|ee\rangle$  or  $|gg\rangle$ , which as proven in Appendix D can never display entanglement at  $t \rightarrow 0^+$ . We have then considered the initial states  $|eg\rangle$  and  $|ge\rangle$ . We observe that, in both cases, the maximum value of negativity generated during the evolution is higher than the one observed in Figs. 1, 2 and 5, where the choice was  $\rho_S(0) = \rho_C$ . Curiously, the sufficient conditions of Appendix D also suggest that these states have, in general, a stronger power of generating entanglement at  $t \rightarrow 0^+$ . Moreover, we observe that the asymmetry between qubit 1 and qubit 2 is reflected in the behavior of  $\mathcal{N}_M$  as a function of the detuning: for instance, if we start the dynamics in  $|eg\rangle$  we find stronger entanglement for  $\Delta\omega > 0$ , and viceversa. In all the other scenarios the behavior of  $\mathcal{N}_M$  is analogous to the one depicted in the figures of the main text.

## B. An experimental proposal to test our findings

We propose here an experimental platform that would allow one to test our predictions in a controllable environment and beyond mathematical approximations, eventually also allowing for the exploration of further regimes. The phenomena we have discussed can be observed by using two superconducting qubits, in a simple experiment as depicted in Fig. 3: two transmon qubits of frequency  $\omega_1$  and  $\omega_2$  are coupled to the same resistor through the capacitors  $C_L$  and  $C_R$ . Let us assume that the qubits have total capacitances (shunt plus intrinsic junction capacitance)  $C_1$  and respectively  $C_2$ . In the weak coupling limit  $C_L, C_R \ll C_1, C_2$ , using standard quantum network analysis in the presence of dissipation [94], we obtain the Hamiltonian Eq. (1). Here the resistor plays the role of a thermal bath with an Ohmic spectral density proportional to the resistance  $R$ . The parameters  $\mu$ ,  $g_1$  and  $g_2$  can be tuned by varying the values of the capacitors in the circuit. Indeed, we obtain:

$$g_1 = \frac{C_L(C_1 + C_2)}{(C_L + C_1)(C_L + C_R)}, \quad (17)$$

$$g_2 = \frac{C_R(C_1 + C_2)}{(C_R + C_2)(C_L + C_R)},$$

and  $\mu$  is a constant with the units of energy, proportional to the resistance and to  $(C_L + C_R)/(C_1 + C_2)$ , that with the above assumption satisfies the weak coupling limit. The temperature of the thermal bath is the effective temperature at which the resistor is dissipating energy, typically some tens of millikelvin.

Let us consider a specific set of parameters: according to the discussion in the previous section, synchronization and subradiance are good signatures of entanglement generation in the balanced case, i.e.  $g_1 = g_2$ . To obtain so, we choose  $C_L$  and  $C_R$  such that  $C_L/(C_L + C_1) = C_R/(C_R + C_2)$ . As reasonable qubit frequencies, we choose  $\omega_1 = 2\pi \times 5$  GHz and  $\omega_2 = 2\pi \times 4.95$  GHz, so  $\Delta\omega = 0.01\omega_1 = 2\pi \times 0.05$  GHz. We set the inverse temperature  $\beta$  such that  $\hbar\omega_1\beta = 10$ , i.e.  $\beta \approx 3 \times 10^{24} J^{-1}$ . This is reasonable, considering that it corresponds to a temperature  $T \approx 24$  mK. Besides, by suitably tuning the magnitude of the coupling capacitances and resistance, we choose the coupling constant  $\mu = 10^{-1.5}\hbar\omega_1 \approx h \times 0.16$  GHz. Finally, taking into account the values which are usually measured in real experiments with transmon qubits [7], we set the local relaxation time as  $T_1 = 3 \times 10^5 / \omega_1 \approx 10 \mu s$ .

We can now investigate the open dynamics of the transmon qubits under the action of the resistor, with the parameters set as above, for the two different initial states associated to the figures of merit of synchronization and subradiance, so as to be able to track the evolution of respectively  $\sigma_{1,2}^x(t)$  and  $P_{1,2}^e(t)$ . The complete information about these observables is acquired by local measurements on each qubit using the standard dispersive scheme. In this scheme,  $P_{1,2}^e(t)$  are obtained directly as populations of the excited state, while for measuring  $\sigma_{1,2}^x(t)$  we need to apply an  $X$ -pulse before the measurement. After performing these measurements, we can compute the synchronization and subradiance measures  $Syn$  and

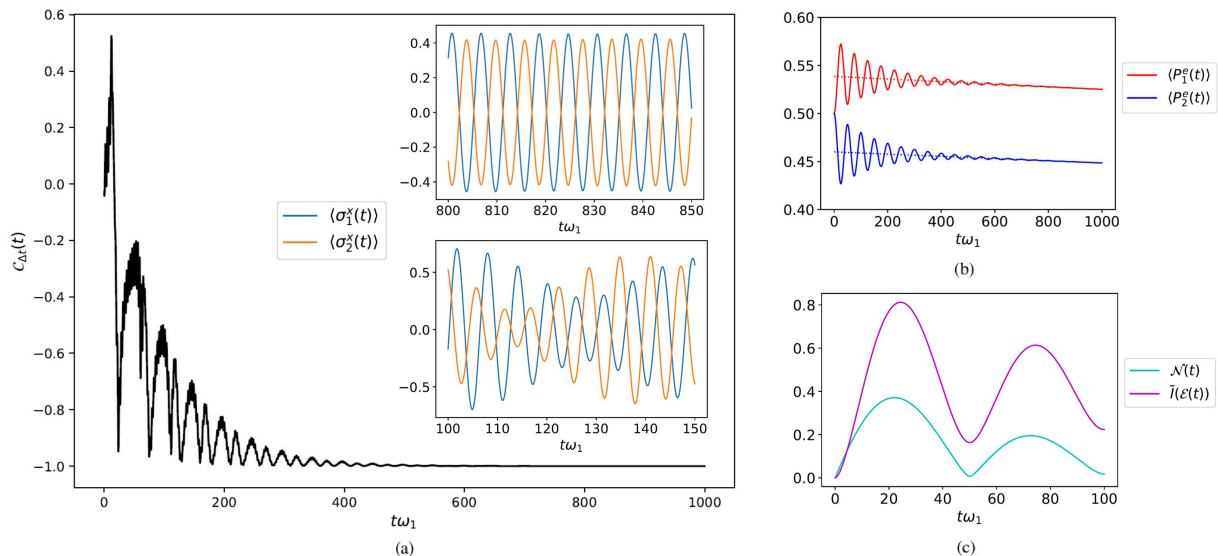


FIG. 4. Evolution of different figures of merit in the scenario discussed in Sec. IV B. (a): Pearson coefficient as a function of time, with  $\Delta t = 7/\omega_1 \approx 0.2 ns$ . The insets depict the evolution of  $\langle \sigma_1^x(t) \rangle$  and  $\langle \sigma_2^z(t) \rangle$  in different time intervals. (b): Dynamics of  $\langle P_1^e(t) \rangle$  (solid red) and  $p_{06}^{(0)} h_{61}^{(0)} + p_{05}^{(0)} h_{51}^{(0)} e^{\lambda_5^{(0)} t}$  (dotted red) for qubit 1, and  $\langle P_2^e(t) \rangle$  (solid blue) and  $p_{06}^{(0)} h_{62}^{(0)} + p_{05}^{(0)} h_{52}^{(0)} e^{\lambda_5^{(0)} t}$  (dotted blue) for qubit 2. The coefficients  $p_{0j}^{(0)}$  and  $h_{jk}^{(0)}$  are defined in Eq. (9), and their combinations (dotted lines) represent the decays of the subradiant mode of each qubit as a function of time. (c): Evolution of negativity  $\mathcal{N}(t)$  and collectiveness  $\bar{I}(\mathcal{E}(t))$ .

*Sub* as discussed in Sec. III. The results of our simulation are plotted in Fig. 4, where we also compare them with the negativity and collectiveness as a function of time (subfig. (c)). The Pearson coefficient depicted in Fig. 4(a) shows the appearance of an antisynchronized regime (upper inset) after an incoherent transient (lower inset). Still, it does not correctly detect the synchronization time  $t_S$  defined in Eq. (C2), since it provides a value higher than 99% for  $t \approx 4.2 \times 10^2/\omega_1$ . On the contrary, a more accurate spectral analysis shows that the time at which the slowest decaying mode in the dynamics of  $\langle \sigma_{1,2}^x(t) \rangle$  is 100–times bigger than all the other ones is  $t_S \approx 8.3 \times 10^2/\omega_1$ , highlighting how the Pearson coefficient alone is not enough accurate to extract the value of *Syn*. Fig. 4(b) depicts the decay of  $\langle P_{1,2}^e(t) \rangle$  as a function of time. We observe the emergence of a subradiant mode which remains alive also at late times, and a spectral analysis reveals the subradiance time Eq. (C4)  $t_B \approx 3.4 \times 10^2/\omega_1$ . From this analysis, we extract the value of the figures of merit  $Syn \approx 428$ ,  $Sub \approx 529$ , according to Eqs. (7) and (10). Finally, let us focus on the negativity and collectiveness in Fig. 4(c):  $\mathcal{N}(t)$  increases at  $t \rightarrow 0^+$ , showing that entanglement is generated as soon as the dynamics begins, as predicted in Appendix D. After having reached a maximum at  $t \approx 21/\omega_1$ , it decreases toward the zero value. Then, a less intense re-birth of entanglement is observed around  $t \approx 50/\omega_1$ , as already predicted in similar models [49]. The collectiveness displays a similar behavior, reaching the top at later times  $t \approx 25/\omega_1$ , and then decreasing with an oscillating behavior. Consistently with the original paper [25], it decays toward 0 at infinite time. From the evolution we obtain the values  $\mathcal{N}_M \approx 0.37$  and  $\bar{I}_M \approx 0.81$ . It is important to note that all

these characteristic times are smaller than the relaxation time  $T_1$ ; this gives a realistic temporal window for performing measurements and observing these effects.

## V. CONCLUSIONS

In this work we have investigated the behavior of quantum synchronization, subradiance, entanglement, and collectiveness of the dynamics, in a broad scenario of two superconducting transmon qubits dissipating into a common thermal bath. Although the four phenomena are essentially different, and a general one-to-one correspondence between them cannot be established, they share a common cause, namely the action of the collective bath. Inspired by this, we have addressed in which scenarios synchronization and subradiance (equipped with well-defined, time-independent quantifiers) can act as signatures of entanglement generation. We also have compared synchronization and subradiance with a measure of the *collectiveness* of the evolution, i.e. of how much the dynamics differs from one described by two separable quantum maps acting locally on each qubit. Finally, we have provided an experimental proposal for a system of two transmon qubits coupled to the same resistor, which mimics a thermal bath.

We have found that quantum synchronization acts as a perfect signature of entanglement generation, i.e. the behavior of its measure varies in the same way of the measure of entanglement production as a function of the model parameters, except in the scenario with the qubits coupled to the bath in an unbalanced way, which favors the emergence of a slowly-decaying eigenmode, while it decreases the collectiveness of the dy-

namics. The measure of subradiance follows the same behavior, but it fails to describe entanglement generation for high temperatures, where the slowly-decaying subradiant eigenmode is not affected by temperature, while the decay rate of all the other modes are enhanced.

Our results also shed new light on the relation between entanglement generation and collectiveness. We have observed that, at least if the initial state of the system is symmetric with respect to the switching of the two qubits, their values follow exactly the same behavior, with the only exception that the collectiveness decreases but does not reach a null value for  $T \rightarrow \infty$ , while entanglement does. Our findings seem to suggest that the two measures are closely related, and a tighter connection between them may be found. Besides, our analysis establishes quantitatively the correlated dissipation strength needed for a pair of transmon qubits to display effects such as entanglement and spontaneous synchronization.

Remarkably, the advantage of employing synchronization or subradiance as signatures of entanglement generation consists in the fact that their measures can be computed by monitoring the mean value as a function of time of local observables only, without relying on joint measurements, which are on the contrary necessary to calculate any measure of entanglement, such as the negativity. We expect this to be especially useful when the system tomography is not available. In particular, it would be interesting to extend our results to systems of multiple qubits which realize a quantum computing platform, for which tomography is not feasible anymore. Furthermore, the experimental proposal we discuss may be implemented with the currently available technology and know-how about superconducting qubits. Its realization would be the first demonstration of spontaneous quantum synchronization, which do not require the presence of an external driving field, in the deep quantum regime.

## ACKNOWLEDGMENTS

The numerical analyses have been performed with the assistance of QuTiP, the Quantum Toolbox in Python [95]. MC acknowledges funding from Fondazione Angelo della Riccia and from the Finnish Center of Excellence in Quantum Technology QTF (project 312296). GSP acknowledges the project QUARTET (grant agreement number 862644, FET Open EU Horizon 2020 research and innovation programme) and the Academy of Finland RADDESS project 328193. Financial support from MINECO/AEI/FEDER through projects EPheQuCS FIS2016-78010-P, CSIC Research Platform PTI-001, the PIE project 202050E098, the project QUAREC funded by CAIB, and the María de Maeztu Program for Units of Excellence in R&D (MDM-2017-0711) is acknowledged.

## Appendix A: Coefficients of the master equation

We assume that the bath is in a thermal state at temperature  $T$ . The coefficients of the master equation (2) read:

$$\begin{aligned}\gamma_{jk}^\downarrow &= g_j g_k (\Gamma_\beta(\omega_j) + \Gamma_\beta(\omega_k)^*) + 1/T_1 \delta_{jk}, \\ \gamma_{jk}^\uparrow &= g_j g_k (\Gamma_\beta(-\omega_j) + \Gamma_\beta(-\omega_k)^*), \\ s_{jk}^\downarrow &= g_j g_k (\Gamma_\beta(\omega_j) - \Gamma_\beta(\omega_k)^*)/2i, \\ s_{jk}^\uparrow &= g_j g_k (\Gamma_\beta(-\omega_j) - \Gamma_\beta(-\omega_k)^*)/2i,\end{aligned}\tag{A1}$$

where  $\Gamma_\beta(\omega)$  is the one-side Fourier transform of the autocorrelation functions of the bath, which depends on the spectral density Eq. (A3) and on the temperature of the thermal bath through  $\beta = 1/k_B T$  [48, 49]:

$$\begin{aligned}\Gamma_\beta(\omega) &= \pi(N_\beta(\omega) + 1)J(\omega) \\ &+ i\mathcal{P} \int_0^\infty d\omega'_k J(\omega'_k) \left( \frac{N_\beta(\omega'_k) + 1}{\omega - \omega'_k} + \frac{N_\beta(\omega'_k)}{\omega + \omega'_k} \right),\end{aligned}\tag{A2}$$

where  $N_\beta(\omega) = \frac{1}{e^{\beta\hbar\omega} - 1} = \frac{1}{2} \left( \coth \frac{\beta\hbar\omega}{2} - 1 \right)$ , and  $J(\omega)$  is the spectral density of the bath, defined as:

$$J(\omega) = \frac{\mu^2}{\hbar^2} \sum_k f_k^2 \delta(\omega - \Omega_k),\tag{A3}$$

where  $f_k$  are introduced in Eq. (1). In the analysis of Sec. IV we have employed an Ohmic spectral density, i.e.:

$$J(\omega) = \frac{\mu^2}{\hbar^2 \omega_1^2} \frac{\omega \omega_C^2}{\omega_C^2 + \omega^2},\tag{A4}$$

where  $\omega_C$  is a cut-off frequency that we have set as  $\omega_C = 20\omega_1$ , and we have chosen to renormalize the spectral density by the frequency of the first qubit.

In the decay coefficients of Eq. (A1) we have added a local dissipative decay rate  $1/T_1$  on each qubit, which represents the action of a phenomenological local bath at zero temperature. Its effects are therefore not relevant for the absorption coefficients, and we have also neglected its contribution to the Lamb-shift. These choices are motivated by the experimental decay observed in a single superconducting qubit, which reaches to a good approximation the ground state at infinite time, corresponding to a thermal bath at zero temperature. On the contrary, we allow for the common bath to have a finite temperature, which experimentally can be realized by local heating of the resistor connecting the qubits.

## Appendix B: Blocks of the Liouvillian superoperator

The master equation (2) is in partial secular approximation and therefore a fundamental symmetry on the superoperator level emerges [50]:  $[\mathcal{L}, \mathcal{N}] = 0$ , where  $\mathcal{N} = [P_1^e + P_2^e, \cdot]$  is the *number superoperator* ( $P_1^e$  and  $P_2^e$  are defined in Eq.(8)). For this reason, the Liouvillian

superoperator can be block-diagonalized with each block labeled by a different eigenvalue of  $\mathcal{N}$ . Let us work in the basis of the space of operators  $\{|jk\rangle\langle lm|\}_{j,k,l,m=e,g}$ .  $\mathcal{N}$  is diagonal in this basis, and its eigenvalues correspond to the number of excited qubit states in the ket minus the number of excited qubit states in the bra. Therefore, a single eigenvalue  $d$  can assume the values  $d = -2, -1, 0, 1, 2$ , and the Liouvillian superoperator is divided into five independent blocks labeled by  $d$ :  $\mathcal{L} = \bigoplus_{d=-2}^2 \mathcal{L}_d$ . In particular, the block  $\mathcal{L}_0$  will act on the basis vectors  $|ee\rangle\langle ee|, |eg\rangle\langle eg|, |eg\rangle\langle ge|, |ge\rangle\langle eg|, |eg\rangle\langle eg|, |gg\rangle\langle gg|$ ,  $\mathcal{L}_1$  on  $|ee\rangle\langle eg|, |ee\rangle\langle ge|, |eg\rangle\langle gg|, |ge\rangle\langle gg|$ ,  $\mathcal{L}_{-1}$  on  $|eg\rangle\langle ee|, |ge\rangle\langle ee|, |gg\rangle\langle eg|, |gg\rangle\langle ge|$ ,  $\mathcal{L}_2$  on  $|ee\rangle\langle gg|$  and  $\mathcal{L}_{-2}$  on  $|gg\rangle\langle ee|$ . In these bases, we have that  $\mathcal{L}_{-1} = \mathcal{L}_1^*$  and  $\mathcal{L}_{-2} = \mathcal{L}_2^*$  (more details in Refs. [50, 51]). The spectral analysis of each block of the Liouvillian superoperator leads to the solution of the dynamics as given by Eq. (5).

## Appendix C: Derivation of the figures of merit

### 1. Quantum synchronization

The Pearson coefficient is defined in a temporal window  $\Delta t$  as:

$$C_{\Delta t}(t) = \frac{\int_t^{t+\Delta t} (\sigma_1^x(t') - \bar{\sigma}_1^x)(\sigma_2^x(t') - \bar{\sigma}_2^x) dt'}{\sqrt{\int_{k=1}^2 \int_t^{t+\Delta t} (\sigma_k^x(t') - \bar{\sigma}_k^x)^2 dt'}}, \quad (\text{C1})$$

where  $\bar{\sigma}_k^x = \frac{1}{\Delta t} \int_t^{t+\Delta t} \sigma_k^x(t') dt'$ . In a scenario in which the dynamics of the observables reaches the perfect in-phase synchronization at a given time  $t_S$ , we observe that the value of the Pearson coefficient stabilizes to 1 at the same time, for a suitable time window  $\Delta t$  [52, 55, 93]. A slightly different definition of the Pearson coefficient allows us to catch the emergence of synchronization with a given phase shift [32].

Let us now focus on a time-independent measure of quantum synchronization. It will depend only on the separation between the real part of the eigenvalues of the modes of  $\mathcal{L}_1$ , on each corresponding inner product  $c_{jk}^{(1)}$  and on the initial conditions, i.e. on the state at which we initialize the system at  $t = 0$ . We start the dynamics from the state  $\rho_S(0) = |\psi_{Syn}\rangle\langle\psi_{Syn}|$  defined in Sec. III A, and we monitor the observables  $\sigma_1^x(t)$  and  $\sigma_2^x(t)$ . The free evolution of each qubit would give  $\langle\sigma_k^x(t)\rangle = \cos(\omega_k t + \phi_k)$  where  $\phi_k$  is a phase depending on the initial conditions, while the presence of a common bath can lead to the synchronization of their dynamics, i.e. to a situation in which they oscillate at the same frequency. To do so, their evolution must be monochromatic, that is to say, the main contribution to the mean value of  $\sigma_k^x(t)$  in Eq. (6) must be given by a single eigenmode of the Liouvillian block  $\mathcal{L}_1$  only. This happens when all the other modes have disappeared due to their faster decay. Let us say that synchronization emerges at the time  $t_S$ , when the contribution of the slowest-decay mode with eigenvalue  $\lambda_4^{(1)}$  to  $\langle\sigma_1^x(t)\rangle$  and  $\langle\sigma_2^x(t)\rangle$  is 100-times bigger than the one of any other mode. Intuitively, at  $t_S$  the Pearson coefficient will have

reached a value  $C_{\Delta t}(t_S) > 0.99$ . Using the notation introduced in Eq. (6), the synchronization time  $t_S$  is estimated by inverting

$$\left| p_{04}^{(1)} c_{4k}^{(1)} \right| e^{\text{Re}(\lambda_4^{(1)})t_S} = 100 \cdot \left| p_{0j}^{(1)} c_{jk}^{(1)} \right| e^{\text{Re}(\lambda_j^{(1)})t_S},$$

and then maximizing over  $j = 2, 3, 4$  and  $k = 1, 2$ . Finally, we get:

$$t_S = \max_{j=1,2,3;k=1,2} \frac{\log\left(\frac{100|p_{0j}^{(1)}c_{jk}^{(1)}|}{|p_{04}^{(1)}c_{4k}^{(1)}|}\right)}{\text{Re}(\lambda_4^{(1)}) - \text{Re}(\lambda_j^{(1)})}. \quad (\text{C2})$$

We observe that the synchronization time depends on the separation between the slowest decay rate and all the other ones, and on the inner product between the eigenvector of the slowest-decaying mode and the initial state,  $\sigma_1^x(t)$  and  $\sigma_2^x(t)$ .

If the two slowest decay rates do not coincide, there will always be a finite synchronization time at which the mean values of the qubit observables will oscillate at the same frequency. However, decoherence appears along the evolution and the synchronization time may be way longer than the time at which the system has lost all of its coherences, and the detection of synchronization would be almost impossible. To take into account the two phenomena, we define the figure of merit of synchronization as the ratio between the synchronization time and the time at which the slowest-decaying mode is reduced to 1/100 of its initial value, and we obtain Eq. (7):

$$Syn = \left| \frac{\log 100}{t_S \text{Re}(\lambda_4^{(1)})} \right|. \quad (\text{C3})$$

Experimentally,  $Syn$  can be estimated by monitoring the mean value of  $\sigma_1^x(t)$  and  $\sigma_2^x(t)$  until the time in which the spectral density of the signal reveals the presence of a single mode only, with an error of the 1%. Then, the decay rate of the remaining mode can be found through an exponential fit of the carrier wave. The higher  $Syn$ , the easier will be to detect quantum synchronization, since the signals of the mean value of  $\sigma_1^x(t)$  and  $\sigma_2^x(t)$  will be more intense at the synchronization time. If  $Syn = 1$ , then the synchronization appears exactly when the only remaining mode is reduced to 1/100 of its initial value.

### 2. Subradiance

The derivation of the figure of merit for subradiance is analogous to the one of quantum synchronization: we want to identify a collective slowly-decaying mode of the system decay which remains alive when all the other modes have vanished. The only differences consist in the observables we want to monitor, that now are  $P_1^e(t)$  and  $P_2^e(t)$  instead of  $\sigma_1^x(t)$  and  $\sigma_2^x(t)$ , and in the initial conditions, that read  $\rho_S(0) = \frac{(|eg\rangle - |ge\rangle)(\langle eg| - \langle ge|)}{2}$ .

In a scenario without a collective bath acting on both the qubits, each of them would decay with an independent decay

rate. On the contrary, the presence of a common bath creates a slowly-decaying collective mode whose component in both  $P_1^e(t)$  and  $P_2^e(t)$  survives after all the other ones have vanished, apart from the mode pertaining to the steady state which does not decay at all (say the one with eigenvalue  $\lambda_6^{(0)} = 0$ ). We want to identify the long-surviving component, let us say corresponding to the eigenvalue  $\lambda_5^{(0)}$ , and the time at which it emerges. Following the discussion about quantum synchronization, we choose the subradiance time  $t_B$  as the time at which the slowest-decaying component in the mean value of  $P_1^e(t_B)$  and  $P_2^e(t_B)$  is 100-times bigger than that of any other mode (apart from the steady state one). Using Eq.(9) and analogously to Eq.(C2), we have:

$$t_B = \max_{j=1,2,3,4;k=1,2} \frac{\log\left(\frac{100|p_{0j}^{(0)}h_{jk}^{(0)}|}{|p_{05}^{(0)}h_{5k}^{(0)}|}\right)}{\text{Re}(\lambda_5^{(0)}) - \text{Re}(\lambda_j^{(0)})}. \quad (\text{C4})$$

As for the case of quantum synchronization, we define the figure of merit of subradiance as the ratio between the subradiance time  $t_B$  and the time at which the component of the slowest-decaying mode  $\lambda_5^{(0)}$  is reduced to 1/100 of its initial value, and we obtain Eq. (10).

Noticing that  $\mathcal{T}_2[A \otimes B\rho] = A \otimes \mathbb{I} \mathcal{T}_2[\rho] \mathbb{I} \otimes B^T$  and  $\mathcal{T}_2[\rho A \otimes B] = \mathbb{I} \otimes B^T \mathcal{T}_2[\rho] A \otimes \mathbb{I}$ , the form of  $\tilde{\mathcal{L}}$  can be derived from Eq. (2) and reads:

$$\begin{aligned} \tilde{\mathcal{L}}[\rho] = & -\frac{i}{2}[(\hbar\omega_1 + s_{11})\sigma_1^z - (\hbar\omega_2 + s_{22})\sigma_2^z, \rho] - i(s_+(\sigma_1^- \rho \sigma_2^- - \sigma_2^- \rho \sigma_1^-) + s_-(\sigma_1^+ \rho \sigma_2^+ - \sigma_2^+ \rho \sigma_1^+)) \\ & + \sum_{j=1,2} \left[ \gamma_{jj}^\downarrow \left( \sigma_j^- \rho \sigma_j^+ - \frac{1}{2} \{ \rho, \sigma_j^+ \sigma_j^- \} \right) + \gamma_{jj}^\uparrow \left( \sigma_j^+ \rho \sigma_j^- - \frac{1}{2} \{ \rho, \sigma_j^- \sigma_j^+ \} \right) \right] + \gamma_{12}^\downarrow \sigma_1^- \sigma_2^- \rho + \gamma_{12}^\uparrow \sigma_1^+ \sigma_2^+ \rho \\ & - \frac{\gamma_{12}^\downarrow + \gamma_{21}^\uparrow}{2} (\sigma_1^- \rho \sigma_2^- + \sigma_2^- \rho \sigma_1^-) - \frac{\gamma_{21}^\downarrow + \gamma_{12}^\uparrow}{2} (\sigma_1^+ \rho \sigma_2^+ + \sigma_2^+ \rho \sigma_1^+) + \gamma_{21}^\downarrow \rho \sigma_1^+ \sigma_2^+ + \gamma_{21}^\uparrow \rho \sigma_1^- \sigma_2^-, \end{aligned} \quad (\text{D1})$$

with  $s_+ = s_{12}^\downarrow + s_{21}^\uparrow$ ,  $s_- = s_{12}^\uparrow + s_{21}^\downarrow$ .

We write the separable state  $\rho$  as  $\rho = |\psi\rangle\langle\psi| \otimes |\varphi\rangle\langle\varphi|$ . Then,  $\tilde{\rho} = |\psi\rangle\langle\psi| \otimes |\varphi^*\rangle\langle\varphi^*|$ , where  $|\varphi^*\rangle$  is the state whose components in the canonical basis of  $\sigma_2^z$  are the complex conjugate of the ones of  $|\varphi\rangle$ . We now have to find a suitable vector  $|\Phi\rangle \in \mathbb{C}_4$  with  $\langle\Phi|\tilde{\rho}|\Phi\rangle = 0$ . The latter condition tells us that we need to choose it in the orthogonal component of the subspace generated by the state  $|\Psi_1\rangle = |\psi\rangle \otimes |\varphi^*\rangle$ , and a suitable basis is expressed as  $|\Psi_2\rangle = |\psi\rangle \otimes |\varphi_{\perp}^*\rangle$ ,  $|\Psi_3\rangle = |\psi_{\perp}\rangle \otimes |\varphi^*\rangle$ ,  $|\Psi_4\rangle = |\psi_{\perp}\rangle \otimes |\varphi_{\perp}^*\rangle$ . Let us define the matrix  $M_{ij} = \langle\Psi_i|\tilde{\mathcal{L}}[\tilde{\rho}|\Psi_j\rangle$ . Then, it is sufficient [89] that  $M_{22}M_{33} < |M_{23}|^2$  for the bath to create entanglement between the qubits at time  $t \rightarrow 0^+$ , starting from  $\rho_S(0) = \rho$ . We now consider different initial conditions and discuss their consequences:

- If  $\rho_S(0) = |gg\rangle\langle gg|$  or  $\rho_S(0) = |ee\rangle\langle ee|$ , we have  $M_{23} = 0$  and  $M_{22}, M_{33} > 0$  for any  $T > 0$ , therefore  $\lim_{t \rightarrow 0^+} \rho_S(t)$  would still be separable in any scenario.

Analogously to the estimation of the figure of merit of quantum synchronization, in order to compute the value of the subradiance measure Eq. (10) in a real experiment one has to track the signals of the mean values  $\langle P_1^e(t) \rangle$  and  $\langle P_2^e(t) \rangle$ . In this way, we are able to detect the time  $t_B$  in which one single decaying component of the signals is 100-times bigger than any other one (after having removed the steady-state one), and to estimate the corresponding decay rate.

#### Appendix D: Sufficient conditions for the entangling power of the bath

We follow the discussion in Ref. [89] in order to provide some sufficient conditions assuring that the master equation (2) has the capability of producing entanglement for some values of its coefficients.  $\mathcal{T}_2$  represents the partial transpose with respect to the qubit 2. According to the partial transpose criterion [90], a two-qubit state  $\rho$  is entangled if and only if  $\tilde{\rho} = \mathcal{T}_2[\rho]$  is negative-definite. Let us define  $\tilde{\mathcal{L}} = \mathcal{T}_2 \circ \mathcal{L} \circ \mathcal{T}_2$ , then we observe that  $\tilde{\mathcal{L}}[\tilde{\rho}] = \mathcal{T}_2[\mathcal{L}[\rho]]$ . It can be shown [89] that a semigroup driven by  $\mathcal{L}$  is entangling if there exist a separable pure state  $\rho$  and a vector  $|\Phi\rangle \in \mathbb{C}_4$  such that  $\langle\Phi|\tilde{\rho}|\Phi\rangle = 0$  and  $\langle\Phi|\tilde{\mathcal{L}}[\tilde{\rho}]|\Phi\rangle < 0$ .

- If  $\rho_S(0) = |ge\rangle\langle ge|$ , the sufficient condition for generating entanglement at time  $t \rightarrow 0^+$  reads  $\gamma_{22}^\downarrow \gamma_{11}^\uparrow < \left(\frac{\gamma_{12}^\downarrow + \gamma_{21}^\uparrow}{2}\right)^2 + s_+^2$ . In particular, we see that the bath always generates entanglement if  $T = 0$ . In any case, we observe that the quantity  $s_+^2$  is relevant to provide a general sufficient condition for the bath to be entangling. An analogous result is found for  $\rho_S(0) = |eg\rangle\langle eg|$ .
- If  $\rho_S(0) = \rho_C = 1/4 \sum_{j,k,l,m=e,g} |jk\rangle\langle lm|$ , i.e. the state we choose as initial state of the evolution in our analysis, as discussed in Sec. III C, the condition is  $(\gamma_{22}^\downarrow + \gamma_{22}^\uparrow)(\gamma_{11}^\downarrow + \gamma_{11}^\uparrow) < \left(\frac{\gamma_{12}^\downarrow + \gamma_{12}^\uparrow + \gamma_{21}^\downarrow + \gamma_{21}^\uparrow}{2}\right)^2 + (s_+ + s_-)^2$ . Once again, we recognize the important role the Lamb-shift terms  $s_{\pm}$  play in assuring a sufficient condition to generate entanglement.

Note that, a priori, if for an initial state we find that entanglement is not generated at time  $t \rightarrow 0^+$ , this does not mean

that entanglement will never appear during its evolution. Indeed, it may be the case that, after a certain time  $t^*$ , the state is represented by a density matrix  $\rho$  for which the condition  $M_{22}M_{33} < |M_{23}|^2$  is verified. In other words, the method we have followed [89] is useful to provide sufficient conditions, while in order to find a necessary one we would need to check that  $M_{22}M_{33} > |M_{23}|^2$  for any initial separable pure state. Furthermore, this procedure does not give any information about the strength of the generated entanglement. To compute it, we need to study the evolution of the state and to find the maximum value of the negativity (see Eq. (12)), as we

have done in Sec. IV.

### Appendix E: Results in further ranges of parameters

In Fig. 5 we plot the value of the measures of quantum synchronization, subradiance, entanglement and collectiveness in different scenarios which extend the analysis of Figs. 1 and 2. Specifically, we vary the detuning and the local dissipative time in subfigures (a)-(d), the coupling constant and the temperature in subfigures (e)-(h) and the temperature and the weights of the coupling in subfigures (i)-(l). The results are discussed in Sec. IV A.

- 
- [1] M. H. Devoret and R. J. Schoelkopf, *Science* **339**, 1169 (2013).
  - [2] G. Wendin, *Rep. Prog. Phys.* **80**, 106001 (2017).
  - [3] F. Arute, K. Arya, R. Babbush, D. Bacon, J. C. Bardin, R. Barends, R. Biswas, S. Boixo, F. G. Brandao, D. A. Buell, *et al.*, *Nature* **574**, 505 (2019).
  - [4] E. Paladino, L. Faoro, G. Falci, and R. Fazio, *Phys. Rev. Lett.* **88**, 228304 (2002).
  - [5] J. M. Martinis and A. Megrant, arXiv preprint:1410.5793 (2014).
  - [6] S. M. Girvin, in *Quantum Machines: Measurement and Control of Engineered Quantum Systems* (Oxford University Press, 2014) pp. 113–256.
  - [7] J. J. Burnett, A. Bengtsson, M. Scigliuzzo, D. Niepce, M. Kudra, P. Delsing, and J. Bylander, *Npj Quantum Inf.* **5**, 54 (2019).
  - [8] J. Koch, T. M. Yu, J. Gambetta, A. A. Houck, D. I. Schuster, J. Majer, A. Blais, M. H. Devoret, S. M. Girvin, and R. J. Schoelkopf, *Phys. Rev. A* **76**, 042319 (2007).
  - [9] K. Lalumière, B. C. Sanders, A. F. van Loo, A. Fedorov, A. Wallraff, and A. Blais, *Phys. Rev. A* **88**, 043806 (2013).
  - [10] U. von Lüpke, F. Beaudoin, L. M. Norris, Y. Sung, R. Winik, J. Y. Qiu, M. Kjaergaard, D. Kim, J. Yoder, S. Gustavsson, L. Viola, and W. D. Oliver, arXiv preprint:1912.04982 (2019).
  - [11] S. J. Devitt, W. J. Munro, and K. Nemoto, *Rep. Prog. Phys.* **76**, 076001 (2013).
  - [12] L.-M. Duan and G.-C. Guo, *Phys. Rev. A* **59**, 4058 (1999).
  - [13] J. P. Clemens, S. Siddiqui, and J. Gea-Banacloche, *Phys. Rev. A* **69**, 062313 (2004).
  - [14] R. Klesse and S. Frank, *Phys. Rev. Lett.* **95**, 1 (2005).
  - [15] E. Novais and H. U. Baranger, *Phys. Rev. Lett.* **97**, 2 (2006).
  - [16] D. Aharonov, A. Kitaev, and J. Preskill, *Phys. Rev. Lett.* **96**, 1 (2006).
  - [17] T. Hayashi, T. Arimitsu, S. Kitajima, and F. Shibata, *J. Phys. A: Math. Theor.* **40**, F457 (2007).
  - [18] A. Shabani, *Phys. Rev. A* **77**, 022323 (2008).
  - [19] E. Novais, E. R. Mucciolo, and H. U. Baranger, *Phys. Rev. A* **78**, 012314 (2008).
  - [20] C. Cafaro and S. Mancini, *Phys. Rev. A* **82**, 012306 (2010).
  - [21] C. Cafaro and S. Mancini, *Int. J. Quantum Inf.* **09**, 309 (2011).
  - [22] J. Preskill, *Quantum Inf. Comput.* **13**, 0181 (2013).
  - [23] E. Novais and E. R. Mucciolo, *Phys. Rev. Lett.* **110**, 010502 (2013).
  - [24] S. H. Jacobsen and F. Mintert, *J. Phys. A: Math. Theor.* **47** (2014).
  - [25] Á. Rivas and M. Müller, *New J. Phys.* **17**, 062001 (2015).
  - [26] D. Layden, M. Chen, and P. Cappellaro, *Phys. Rev. Lett.* **124**, 020504 (2020).
  - [27] D. Braun, *Phys. Rev. Lett.* **89**, 277901 (2002).
  - [28] G. De Chiara, R. Fazio, C. Macchiavello, and G. M. Palma, *Europhys. Lett.* **67**, 714 (2004).
  - [29] G. De Chiara, R. Fazio, C. Macchiavello, and G. M. Palma, *Int. J. Quantum Inf.* **03**, 207 (2005).
  - [30] S. Filipp, P. Maurer, P. J. Leek, M. Baur, R. Bianchetti, J. M. Fink, M. Göppl, L. Steffen, J. M. Gambetta, A. Blais, and A. Wallraff, *Phys. Rev. Lett.* **102**, 200402 (2009).
  - [31] S. Shankar, M. Hatridge, Z. Leghtas, K. M. Sliwa, A. Narla, U. Vool, S. M. Girvin, L. Frunzio, M. Mirrahimi, and M. H. Devoret, *Nature* **504**, 419 (2013).
  - [32] F. Galve, G. L. Giorgi, and R. Zambrini, in *Lectures on General Quantum Correlations and their Applications* (Springer, 2017) pp. 393–420.
  - [33] A. Crubellier, S. Liberman, D. Pavolini, and P. Pillet, *J. Phys. B: At. Mol. Opt.* **18**, 3811 (1985).
  - [34] T. Bienaimé, N. Piovella, and R. Kaiser, *Phys. Rev. Lett.* **108**, 123602 (2012).
  - [35] M. Gross and S. Haroche, *Phys. Rep.* **93**, 301 (1982).
  - [36] D. Pavolini, A. Crubellier, P. Pillet, L. Cabaret, and S. Liberman, *Phys. Rev. Lett.* **54**, 1917 (1985).
  - [37] R. G. DeVoe and R. G. Brewer, *Phys. Rev. Lett.* **76**, 2049 (1996).
  - [38] W. Guerin, M. O. Araújo, and R. Kaiser, *Phys. Rev. Lett.* **116**, 083601 (2016).
  - [39] D. Bhatti, R. Schneider, S. Oettel, and J. von Zanthier, *Phys. Rev. Lett.* **120**, 113603 (2018).
  - [40] L. Postler, Á. Rivas, P. Schindler, A. Erhard, R. Stricker, D. Nigg, T. Monz, R. Blatt, and M. Müller, *Quantum* **2**, 90 (2018).
  - [41] G. L. Giorgi, F. Galve, and R. Zambrini, *Phys. Rev. A* **94**, 052121 (2016).
  - [42] K. Gibble, *Physics* **3**, 55 (2010).
  - [43] M. Xu, D. A. Tieri, E. C. Fine, J. K. Thompson, and M. J. Holland, *Phys. Rev. Lett.* **113**, 154101 (2014).
  - [44] A. Ronzani, B. Karimi, J. Senior, Y.-C. Chang, J. T. Peltonen, C. Chen, and J. P. Pekola, *Nat. Phys.* **14**, 991 (2018).
  - [45] J. M. Weiner, K. C. Cox, J. G. Bohnet, and J. K. Thompson, *Phys. Rev. A* **95**, 033808 (2017).
  - [46] A. W. Laskar, P. Adhikary, S. Mondal, P. Katiyar, S. Vinjanamathy, and S. Ghosh, arXiv preprint:1910.11832 (2019).
  - [47] M. Koppenhöfer, C. Bruder, and A. Roulet, *Phys. Rev. Res.* **2**, 023026 (2020).

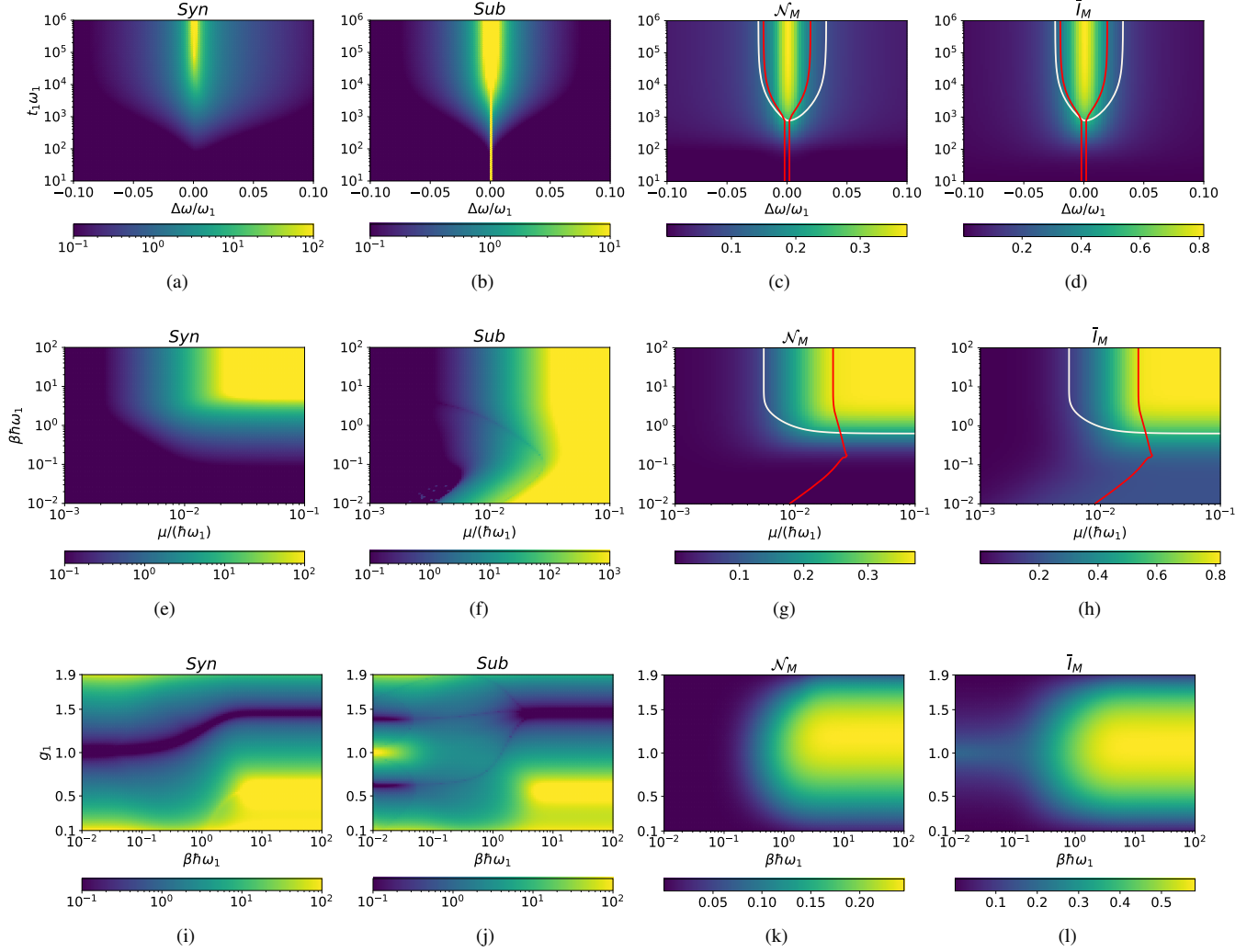


FIG. 5. Measure of quantum synchronization, subradiance, entanglement generation and collectiveness in different ranges of parameters. In figs. (a)-(d) we vary the detuning  $\Delta\omega = \omega_1 - \omega_2$  and the local dissipative time  $T_1$ , having fixed  $\mu = 10^{-2}\hbar\omega_1$ ,  $\beta = 10/\hbar\omega_1$  and  $g_1 = g_2 = 1$ . In Figs. (e)-(h) we vary the coupling constant  $\mu$  vs. the inverse temperature  $\beta$ , with  $\Delta\omega = 0.01\omega_1$ ,  $T_1 = 3 \times 10^5/\omega_1$  and  $g_1 = g_2 = 1$ . In Figs. (i)-(l) we study the unbalanced scenario, varying the weight  $g_1$  (with  $g_2 = 2 - g_1$ ) and the inverse temperature  $\beta$ ; the remaining parameters read  $\mu = 10^{-2}\hbar\omega_1$ ,  $\Delta\omega = 0.01\omega_1$  and  $T_1 = 3 \times 10^5/\omega_1$ . We have chosen an Ohmic spectral density of the environment (see Eq. (A4)). The white line in figs. (c)-(d) and (g)-(h) indicates the parameter region in which  $Syn > 1$ , while the red line delimits the area with  $Sub > 1$  in Figs. (c)-(d) while  $Sub > 100$  in Figs. (g)-(h).

- [48] H.-P. Breuer and F. Petruccione, *The theory of open quantum systems* (Oxford University Press, 2002).
- [49] M. Cattaneo, G. L. Giorgi, S. Maniscalco, and R. Zambrini, *New J. Phys.* **21**, 113045 (2019).
- [50] M. Cattaneo, G. L. Giorgi, S. Maniscalco, and R. Zambrini, *Phys. Rev. A* **101**, 042108 (2020).
- [51] B. Bellomo, G. L. Giorgi, G. M. Palma, and R. Zambrini, *Phys. Rev. A* **95**, 043807 (2017).
- [52] G. L. Giorgi, F. Galve, G. Manzano, P. Colet, and R. Zambrini, *Phys. Rev. A* **85**, 052101 (2012).
- [53] G. Manzano, F. Galve, G. L. Giorgi, E. Hernández-García, and R. Zambrini, *Sci. Rep.* **3**, 1439 (2013).
- [54] A. Mari, A. Farace, N. Didier, V. Giovannetti, and R. Fazio, *Phys. Rev. Lett.* **111**, 6 (2013).
- [55] G. L. Giorgi, F. Plastina, G. Francica, and R. Zambrini, *Phys. Rev. A* **88**, 042115 (2013).
- [56] B. Zhu, J. Schachenmayer, M. Xu, F. Herrera, J. G. Restrepo, M. J. Holland, and A. M. Rey, *New J. Phys.* **17**, 083063 (2015).
- [57] V. Ameri, M. Eghbali-Arani, A. Mari, A. Farace, F. Kheirandish, V. Giovannetti, and R. Fazio, *Phys. Rev. A* **91**, 012301 (2015).
- [58] A. Cabot, F. Galve, and R. Zambrini, *New J. Phys.* **19**, 113007 (2017).
- [59] A. Cabot, F. Galve, V. M. Eguíluz, K. Klemm, S. Maniscalco, and R. Zambrini, *Npj Quantum Inf.* **4**, 57 (2018).
- [60] S. Siwiak-Jaszek and A. Olaya-Castro, *Faraday Discuss.* **216**, 38 (2019).
- [61] A. Cabot, G. L. Giorgi, F. Galve, and R. Zambrini, *Phys. Rev. Lett.* **123**, 023604 (2019).

- [62] G. Karpat, I. Yalçinkaya, and B. Çakmak, *Phys. Rev. A* **100**, 12133 (2019).
- [63] H. Eneriz, D. Z. Rossatto, F. A. Cárdenas-López, E. Solano, and M. Sanz, *Sci. Rep.* **9**, 19933 (2019).
- [64] N. Es'haqi-Sani, G. Manzano, R. Zambrini, and R. Fazio, *Phys. Rev. Res.* **2**, 023101 (2020).
- [65] J. Tindall, C. Sánchez Muñoz, B. Buča, and D. Jaksch, *New J. Phys.* **22**, 013026 (2020).
- [66] G. L. Giorgi, A. Cabot, and R. Zambrini, in *Advances in Open Systems and Fundamental Tests of Quantum Mechanics* (Springer, 2019) pp. 73–89.
- [67] O. V. Zhirov and D. L. Shepelyansky, *Phys. Rev. Lett.* **100**, 014101 (2008).
- [68] T. E. Lee and H. R. Sadeghpour, *Phys. Rev. Lett.* **111**, 234101 (2013).
- [69] S. Walter, A. Nunnenkamp, and C. Bruder, *Phys. Rev. Lett.* **112**, 094102 (2014).
- [70] M. B. Plenio, S. F. Huelga, A. Beige, and P. L. Knight, *Phys. Rev. A* **59**, 2468 (1999).
- [71] A. Beige, S. Bose, D. Braun, S. F. Huelga, P. L. Knight, M. B. Plenio, and V. Vedral, *J. Mod. Opt.* **47**, 2583 (2000).
- [72] A. M. Basharov, *J. Exp. Theor. Phys.* **94**, 1070 (2002).
- [73] M. B. Plenio and S. F. Huelga, *Phys. Rev. Lett.* **88**, 197901 (2002).
- [74] M. S. Kim, J. Lee, D. Ahn, and P. L. Knight, *Phys. Rev. A* **65**, 040101 (2002).
- [75] F. Benatti, R. Floreanini, and M. Piani, *Phys. Rev. Lett.* **91**, 070402 (2003).
- [76] X. X. Yi, C. S. Yu, L. Zhou, and H. S. Song, *Phys. Rev. A* **68**, 052304 (2003).
- [77] B. Kraus and J. I. Cirac, *Phys. Rev. Lett.* **92**, 013602 (2004).
- [78] K. Lendi and A. J. van Wonderen, *J. Phys. A: Math. Theor.* **40**, 279 (2007).
- [79] S. Diehl, A. Micheli, A. Kantian, B. Kraus, H. P. Büchler, and P. Zoller, *Nat. Phys.* **4**, 878 (2008).
- [80] M. Hor-Meyll, A. Auyuanet, C. V. S. Borges, A. Aragão, J. A. O. Huguenin, A. Z. Khoury, and L. Davidovich, *Phys. Rev. A* **80**, 042327 (2009).
- [81] F. Benatti, R. Floreanini, and U. Marzolino, *Phys. Rev. A* **81**, 012105 (2010).
- [82] F. Caruso, A. W. Chin, A. Datta, S. F. Huelga, and M. B. Plenio, *Phys. Rev. A* **81**, 062346 (2010).
- [83] A. Gonzalez-Tudela, D. Martin-Cano, E. Moreno, L. Martin-Moreno, C. Tejedor, and F. J. Garcia-Vidal, *Phys. Rev. Lett.* **106**, 020501 (2011).
- [84] Y.-D. Wang and A. A. Clerk, *Phys. Rev. Lett.* **110**, 253601 (2013).
- [85] F. Reiter, L. Tornberg, G. Johansson, and A. S. Sørensen, *Phys. Rev. A* **88**, 032317 (2013).
- [86] Z. Leghtas, U. Vool, S. Shankar, M. Hatridge, S. M. Girvin, M. H. Devoret, and M. Mirrahimi, *Phys. Rev. A* **88**, 023849 (2013).
- [87] H. Krauter, C. A. Muschik, K. Jensen, W. Wasilewski, J. M. Petersen, J. I. Cirac, and E. S. Polzik, *Phys. Rev. Lett.* **107**, 080503 (2011).
- [88] Y. Lin, J. P. Gaebler, F. Reiter, T. R. Tan, R. Bowler, A. S. Sørensen, D. Leibfried, and D. J. Wineland, *Nature* **504**, 415 (2013).
- [89] F. Benatti, A. M. Liguori, and A. Nagy, *J. Math. Phys.* **49**, 042103 (2008).
- [90] G. Vidal and R. F. Werner, *Phys. Rev. A* **65**, 032314 (2002).
- [91] M. A. Nielsen and I. L. Chuang, *Quantum Computation and Quantum Information: 10th Anniversary Edition* (Cambridge University Press, 2010).
- [92] A. Cabot, G. L. Giorgi, and R. Zambrini, arXiv preprint:1912.10984 (2019).
- [93] G. Karpat, I. Yalçinkaya, and B. Çakmak, *Phys. Rev. A* **101**, 042121 (2020).
- [94] A. Parra-Rodríguez, E. Rico, E. Solano, and I. L. Egusquiza, *Quantum Sci. Technol.* **3**, 024012 (2018).
- [95] J. R. Johansson, P. D. Nation, and F. Nori, *Comput. Phys. Commun.* **184**, 1234 (2013).